

Bragg-Cherenkov resonance and polaron-like decoupling of the Wigner solid on superfluid helium

Yu.P. Monarkha^{1,*}

¹*B. Verkin Institute for Low Temperature Physics and Engineering of the National Academy of Sciences of Ukraine, 47 Nauky Ave., Kharkiv 61103, Ukraine*

Nonlinear polaron-like dynamics of the two-dimensional Wigner solid (WS) on superfluid ⁴He are theoretically analyzed in different models and transport regimes for their similarities and distinctions. The Bragg-Cherenkov (BC) resonant excitation of surface waves and WS decoupling from surface dimples were usually considered in terms of a dc transport model. At the same time, field-velocity characteristics of the WS are measured under ac conditions and presented for time-averaged quantities. Here the nonlinear equation of motion of the WS coupled to surface dimples is studied for ac conditions using two different approaches based on fixing the driving field or the output current. Both approaches are shown to give similar results for the first harmonics of major transport properties. In the ac theory, the BC-resonances for dimple inertia and the momentum relaxation rate have asymmetrical shapes, which is in contrast with the results of dc models. Even a quite low driving frequency is shown to affect the amplitude of the BC resonance and decoupling of the WS. Above the BC threshold, the effective mass of surface dimples as a function of the velocity amplitude strongly oscillates indicating multiple recoupling processes.

PACS numbers: 73.20.Qt, 73.40.-c, 67.90.+z, 71.45.Lr

I. INTRODUCTION

Transport properties of a two-dimensional (2D) Wigner solid on the free surface of superfluid helium have much in common with the polaron dynamics¹. Though electron interaction with capillary wave excitations (ripples) usually is rather weak and the single-electron self-trapping can happen only at ultra-low temperatures, in the Wigner solid (WS) state surface dimples appearing under each electron play a crucial role in the WS dynamics at usual liquid-helium temperatures. Such a dimple lattice (DL) does not affect the WS phase transition because the electron-dimple interaction energy² is much smaller than the typical Coulomb interaction energy $e^2\sqrt{n_e}$ (here n_e is the areal density of electrons). Still, the DL affects electron transport along the surface because the effective mass of a dimple M_D is much larger than the free electron mass m_e . The linear dynamics of the coupled WS-DL system³ had given the possibility to detect⁴ the WS of surface electrons and to establish its structure.

Experimental study of the WS conductivity over the liquid helium surface had revealed a body of remarkable nonlinear phenomena. Firstly, we would like to note a sharp change in the magnetoresistance of surface electrons⁵ attributed to the nonequilibrium melting of the electron crystal. A similar effect presumably of different origin was reported⁶ as an abrupt jump of the ac Corbino conductivity σ_{xx} . A mobility jump was observed also in a zero magnetic field⁷.

By now several theoretical models were proposed to explain the nonlinear conductivity of the WS on superfluid liquid helium. The magneto-conductivity jump observed was attributed to the collective sliding of the electrons out of the periodic deformation of the helium surface (the sliding model)^{6,8}. The Bragg-Cherenkov (BC) scattering

model⁹ describes the saturation of velocity data¹⁰ observed when the Hall velocity v_H approaches the phase velocity of the capillary wave whose wavevector \mathbf{q} coincides with the smallest reciprocal lattice vector \mathbf{g} . Another dc model explaining the Hall-velocity limited magnetoconductivity¹⁰ and the conductivity jumps⁶ is based on the hydrodynamic approach¹¹. In this treatment, the BC effect leads to a resonance increase of the DL depth, and instability appears as a breach of the balance of forces acting on the WS: at a certain velocity, electrons decouple from the DL (the decoupling model). Even though both sliding and decoupling models sometimes are assumed to be physically the same, we would like to emphasize their important distinctions. In the sliding model, an electron overcomes the potential (induced by the dimple) as a function of motion coordinate. In the decoupling model¹¹, the potential induced by the dimple is considered as a function of electron velocity, while the relative displacement of the WS and DL is set to zero.

The above noted theoretical models are proposed for dc transport conditions, while the experiments^{6,7,10} are conducted under ac conditions when the driving electric field E and electron velocity v are periodic functions of time t . The real quantities measured in this case are somehow averaged or represent amplitudes of the field and current. A finite frequency should affect the BC response of liquid media because an electron is in the BC resonance condition for only a limited time. Under ac conditions with a given driving electric field $E(t) = E_a \sin \omega t$ (we shall call it the given-field regime), the equation of motion describing the coupled WS-DL system is a very complicated nonlinear integro-differential equation. The accurate solution of this equation was obtained¹²⁻¹⁴ only for the inverse problem, finding $E(t)$ for a given current $j = j_a \sin \omega t$ (the given-current regime). This approach

surprisingly leads to the bistability of velocity-field characteristics for amplitudes j_a and E_a which can explain mobility jumps observed. It should be noted here that the dc-decoupling model¹¹ can be considered as a particular case of the given-current regime with $j = \text{const}$. Under magnetic field directed perpendicular to the surface, calculated σ_{xx} also exhibits a strong jump and a sharp fall which leads to negative conductivity effects¹⁴. Qualitatively, the efficiency of the inverse solution can be attributed to the fact that in experiments with the WS on liquid helium the driving electric field is often adjusted to the current owing to electron redistribution which screens external potential variations. Nevertheless, by now it was not clear if the effects obtained by solving the inverse problem can correspond to the solution of the nonlinear equation of motion for a given driving field $E(t)$. This question recently becomes of special interest because of new time-resolved measurements on WS transport over the surface of superfluid helium confined in a micron-scale channel^{15–17}. Additional interest in this problem was inspired by similarities between the nonlinear transport properties in the WS-DL system and polaron systems^{18–20}.

In this work, we theoretically analyze different models and approaches used for the description of the nonlinear transport of the WS over the free surface of superfluid helium and compare the results. In particular, we shall show that the accurate treatment of the given-field regime, $E(t) = E_a \sin \omega t$, in the lowest nonlinear approximation confirms the validity of the exact solutions for the dimple-mass M_D and the electron-dimple momentum relaxation rate ν_D found using the given-current regime¹⁴. Therefore, the relationship between amplitudes of the first harmonics of the driving electric field and current obtained in the given-current treatment can be used for explaining experimental results regardless of the actual transport regime. Moreover, concentrating on the low-frequency limit ($\omega \ll \omega_g$, here ω_g is the ripplon spectrum) we found that the effective mass of surface dimples increases with the velocity amplitude at a rate which differs from the rate obtained in the DC models. At the same time, the position and height of the BC-resonance maxima for the dimple mass and momentum relaxation rate are shown to be strongly affected even by a very low frequency usually used in experiments on WS transport.

II. WS-DL COUPLING: NONLINEAR DYNAMICS

Consider a 2D electron lattice on the free surface of superfluid ⁴He at low temperatures $T < 0.4\text{K}$. In this case, electrons interact mostly with surface excitations (ripples) which have capillary-wave dispersion $\omega_q = \sqrt{\alpha/\rho}q^{3/2}$, here α and ρ are the surface tension and mass density of liquid helium, respectively. The DL is described by a periodic surface distortion $\xi(\mathbf{r})$. We shall consider only the spatially uniform driving electric

field $E(t)$ and the WS displacement $u(t)$ directed along the x -axis. Then, in the coupled equations of motion for the Fourier transforms $\xi_{\mathbf{q}}$ (only $\mathbf{q} = \mathbf{g}$ are important) and $u(t)$, the interaction force can be averaged over fast thermal and zero-point vibrations²¹. Finally, equations describing the WS-DL coupling can be presented in the following way

$$\ddot{\xi}_{\mathbf{g}} + 2\gamma_g \dot{\xi}_{\mathbf{g}} + \omega_g^2 \xi_{\mathbf{g}} = -\frac{n_e g}{\rho} \tilde{V}_g e^{-ig_x u(t)} \quad (1)$$

$$m_e \ddot{u} + \sum_{\mathbf{g}} \xi_{\mathbf{g}} \tilde{V}_g i g_x e^{ig_x u(t)} = eE \quad (2)$$

where $\tilde{V}_q = V_q \exp(-q^2 \langle u_f^2 \rangle / 4)$, V_q is the electron-ripplon coupling function defined in Ref. 1 ($V_q \rightarrow eE_{\perp}$ in the limit of strong pressing electric fields E_{\perp}), n_e is the areal electron density, $\langle u_f^2 \rangle$ is the mean-square displacement due to fast modes, and γ_g is the damping coefficient which is extremely small for liquid ⁴He. For typical n_e and $0.4\text{K} > T > 0.1\text{K}$, the ratio γ_g/ω_g varies from 10^{-4} to 10^{-7} . The Debye-Waller factor appears in \tilde{V}_q as a result of averaging over fast vibrations and a self-consistent procedure (for a review see Ref. 21).

Eq. (1) represents a linear oscillator equation affected by an electron pressure depending on $u(t)$. It can be solved quite generally, and the solution $\xi_{\mathbf{g}}(t)$ can be represented in the integral form¹²:

$$\xi_{\mathbf{g}}(t) = -\frac{n_e g \tilde{V}_g}{\rho \hat{\omega}_g} \int_0^{\infty} e^{-\gamma_g \tau} \sin(\hat{\omega}_g \tau) e^{-ig_x u(t-\tau)} d\tau,$$

where $\hat{\omega}_g^2 = \omega_g^2 - \gamma_g^2$. Then, inserting $\xi_{\mathbf{g}}(t)$ into Eq. (2) one can find the final nonlinear equation for $u(t)$

$$m_e \ddot{u} = F_D(u) + eE(t), \quad (3)$$

where

$$F_D(u) = -\sum_{\mathbf{g}} \frac{n_e g \tilde{V}_g^2}{m_e \rho \hat{\omega}_g} g_x \times$$

$$\times \int_0^{\infty} \sin(\hat{\omega}_g \tau) e^{-\gamma_g \tau} \sin\{g_x [u(t) - u(t-\tau)]\} d\tau. \quad (4)$$

The functional $F_D(u)$ represents the average force acting on an electron due to the presence of the DL. If the WS is at rest, this force is obviously zero. When the WS moves along the surface, $F_D(u) \neq 0$ because of a finite ripplon damping (the dimple shape becomes asymmetrical along the x -axis) and the dimple inertia. In the general case, the equation of motion of the coupled WS-DL system represents a nonlinear integro-differential equation whose solution is very difficult to find.

A. The dc modeling of nonlinear effects

It is instructive to consider firstly the dc transport model. In this case, $u(t) = vt$ with $v = \text{const}$, and the integral of Eq. (4) can be evaluated analytically. The dimple inertia can't enter the equation of motion of the dc model ($\ddot{u} = 0$), therefore, it is convenient to rewrite the average force acting on an electron due to the polaronic effect as

$$F_D^{(\text{dc})}(v) = -m_e \nu_D^{(\text{dc})}(v) v, \quad (5)$$

where $\nu_D^{(\text{dc})}(v)$ plays the role of a momentum relaxation rate caused by the interaction with a surface dimple

$$\nu_D^{(\text{dc})}(v) = \sum_{\mathbf{g}} \Gamma_g \frac{g_x^2}{g^2} \omega_g \mathcal{N}_{\text{dc}} \left(\frac{v}{v_{g_x}}, \frac{\gamma_g}{\omega_g} \right), \quad (6)$$

$$\Gamma_g = \frac{n_e g^3 \tilde{V}_g^2}{m_e \rho \omega_g^4}, \quad (7)$$

$$\mathcal{N}_{\text{dc}}(v', \gamma'_g) = \frac{2\gamma'_g}{\left[1 - (v')^2\right]^2 + 4(\gamma'_g v')^2}, \quad (8)$$

and we have used the following notations: $v_{g_x} = \omega_g/g_x$, $v' = v/v_{g_x}$, $\gamma'_g = \gamma_g/\omega_g$. The dimensionless parameter Γ_g represents the strength of the WS-DL coupling. Under usual conditions ($n_e \approx 5 \cdot 10^8 \text{ cm}^{-2}$) it is of the order of 10^2 . Actually the result given in Eqs. (5)-(8) is a 3D extension of the 1D decoupling model¹¹. The equation of motion is reduced to a simple balance equation for the two forces acting on an electron: $F_D^{(\text{dc})}(v) + eE = 0$, where the function $F_D^{(\text{dc})}(v)$ has a maximum when $v/v_{|g_x|}$ is close to 1. If eE exceeds the maximum value of $F_D^{(\text{dc})}(v)$, the balance of forces is impossible and the WS decouples from the DL.

The appearance of the BC resonance of $\mathcal{N}_{\text{dc}}(v', \gamma'_g)$ and $\nu_D^{(\text{dc})}(v)$ is quite obvious because the substitution $u(t) = vt$ makes the right side of Eq. (1) a harmonic force with a frequency $g_x v$ acting on a linear oscillator with its own frequency ω_g . Therefore, in the dc model, the BC resonance is similar to the usual resonance appearing when the frequency of an external force $\omega \rightarrow \omega_g$.

It should be noted that the dimple effective mass does not enter the balance of forces of the dc model. In the real case, to reach the decoupling point one has to increase the driving force and, therefore, it becomes a function of time $eE(t)$. Generally, the electric field can be increased so fast that the DL will not follow the WS, and one can imagine the WS sliding caused by a relative displacement of WS and DL. This is why we prefer to separate the decoupling model from the sliding model.

The effective mass of the DL, $N_e M_D^{(\text{dc})}(v)$, can be found as the associated mass induced by the hydrodynamic velocity field in liquid helium. Using the solution

$\xi_{\mathbf{g}}(t)$ mentioned above, one can find $M_D^{(\text{dc})}(v)$ as

$$\frac{M_D^{(\text{dc})}(v)}{m_e} = \sum_{\mathbf{g}} \Gamma_g \frac{g_x^2}{g^2} \mathcal{M}_{\text{dc}} \left(\frac{v}{v_{g_x}}, \frac{\gamma_g}{\omega_g} \right), \quad (9)$$

where

$$\mathcal{M}_{\text{dc}}(v', \gamma'_g) = \frac{1}{\left[1 - (v')^2\right]^2 + 4(\gamma'_g v')^2} \quad (10)$$

is a dimensionless function. Thus, the dimple mass increases with v similarly to $\nu_D^{(\text{dc})}(v)$ [see Eq. (8)]: $\mathcal{N}_{\text{dc}} = 2\gamma'_g \mathcal{M}_{\text{dc}}$. The limited value $M_D^{(\text{dc})}(0)$ coincides with the result of the linear theory³.

In the decoupling model¹¹, the electron lattice and DL were not relatively displaced until the instability occurs. It is instructive to investigate also stability of the WS-DL coupling concerning small relative displacements. Introducing the displacement parameter b along the x -axis, one can find

$$\frac{F_D^{(\text{dc})}(b)}{m_e} = - \sum_{\mathbf{g}} \Gamma_g \frac{g_x \omega_g^2}{g^2} \mathcal{M}_{\text{dc}} \left(\frac{v}{v_{g_x}}, \frac{\gamma_g}{\omega_g} \right) \times \left\{ \left[1 - \left(\frac{v}{v_{g_x}} \right)^2 \right] \sin(g_x b) + 2 \frac{\gamma_g}{\omega_g} \frac{v}{v_{g_x}} \cos(g_x b) \right\}. \quad (11)$$

Eqs. (5) and (6) can be found from Eq. (11) by setting b to zero. The second term in the curly brackets is a decreasing function of b , but it is much smaller than the first term except for the limiting case $v \rightarrow v_{g_x}$. Considering only a small relative displacement and assuming $\gamma_g/\omega_g \ll 1$, one can represent $F_D^{(\text{dc})}$ as

$$F_D^{(\text{dc})}(b) \simeq -m_e \Omega^2 b, \quad (12)$$

where

$$\Omega^2(v) = \sum_{\mathbf{g}} \frac{g_x^2}{g^2} \frac{\Gamma_g \omega_g^2 \left[1 - \left(\frac{v}{v_{g_x}} \right)^2 \right]}{\left[1 - \left(\frac{v}{v_{g_x}} \right)^2 \right]^2 + 4 \left(\frac{\gamma_g}{\omega_g} \frac{v}{v_{g_x}} \right)^2}. \quad (13)$$

In the linear regime $v \ll v_1^{(\text{bc})}$ (here $v_1^{(\text{bc})}$ is the smallest value of $v_{|g_x|}$), $\Omega(0)$ coincides with the typical frequency of electron oscillations in the bottom of a surface dimple ω_f which is usually much higher than ω_{g_1} . Therefore, at $v < v_1^{(\text{bc})}$ the quantity $\Omega^2 > 0$ and the strong force of Eq. (12) restores the equilibrium position of the electron lattice. On the contrary, at $v > v_1^{(\text{bc})}$ the $\Omega^2(v)$ becomes negative, and the force of Eq. (12) provides an additional drive for WS decoupling from the DL.

B. The ac theory of nonlinear effects for a given-current regime

As noted in the Introduction, the exact solution of Eq. (3) can be found only for a given-current regime considering the harmonic dependence of the WS motion: $u(t) = u_a \sin(\omega t)$. In this treatment, the force acting on an electron due to interactions with the DL can be represented as a sum of harmonics. The first harmonic can be found as¹⁴

$$F_D^{(\text{ac})} = -m_e \nu_D^{(\text{ac})} v_a \cos(\omega t) + M_D^{(\text{ac})} \omega v_a \sin(\omega t), \quad (14)$$

where the functions $\nu_D^{(\text{ac})}(v_a, \omega)$ and $M_D^{(\text{ac})}(v_a, \omega)$ have the same physical meaning as $\nu_D^{(\text{dc})}(v)$ and $M_D^{(\text{dc})}(v)$ introduced above for the dc conditions (here $v_a = \omega u_a$ is the velocity amplitude). Indeed, in the right side of Eq. (14), the first term represents the nonlinear kinetic friction (it is proportional to velocity), while the second term takes into account the dimple inertia (it is proportional to acceleration).

The expressions for $\nu_D^{(\text{ac})}$ and $M_D^{(\text{ac})}$ are found as the Fourier transforms of Eq. (4):

$$\frac{M_D^{(\text{ac})}(v_a)}{m_e} = \sum_{\mathbf{g}} \Gamma_g \frac{g_x^2}{g^2} \mathcal{M}_{\text{ac}} \left(\frac{v_a}{v_{g_x}}, \frac{\omega}{\omega_g}, \frac{\gamma_g}{\omega_g} \right), \quad (15)$$

$$\nu_D^{(\text{ac})}(v_a) = \sum_{\mathbf{g}} \Gamma_g \frac{g_x^2}{g^2} \omega_g \mathcal{N}_{\text{ac}} \left(\frac{v_a}{v_{g_x}}, \frac{\omega}{\omega_g}, \frac{\gamma_g}{\omega_g} \right), \quad (16)$$

where

$$\begin{aligned} \mathcal{M}_{\text{ac}}(v'_a, \omega', \gamma'_g) &= -\frac{2}{\omega' v'_a} \int_0^\infty \sin(x) e^{-\gamma'_g x} \sin\left(\frac{\omega' x}{2}\right) \times \\ &\times J_1 \left(2 \frac{v'_a}{\omega'} \sin\left(\frac{\omega' x}{2}\right) \right) dx, \end{aligned} \quad (17)$$

$$\begin{aligned} \mathcal{N}_{\text{ac}}(v'_a, \omega', \gamma'_g) &= \frac{2}{v'_a} \int_0^\infty \sin(x) e^{-\gamma'_g x} \cos\left(\frac{\omega' x}{2}\right) \times \\ &\times J_1 \left(2 \frac{v'_a}{\omega'} \sin\left(\frac{\omega' x}{2}\right) \right) dx, \end{aligned} \quad (18)$$

$J_1(z)$ is the Bessel function, $v'_a = v_a/v_{g_x}$, and $\omega' = \omega/\omega_g$. Other notations are the same as in Eq. (8). In Eqs. (17) and (18), one can consider only positive values of the parameter $v'_a \propto g_x$ because \mathcal{M}_{ac} and \mathcal{N}_{ac} are independent of the sign of v'_a (g_x). Alternatively, we can redefine $v'_a = v_a/|v_{g_x}|$.

For the given-current regime ($v = v_a \cos \omega t$), the first harmonic of the driving electric field is found from Eq. (3) as $E(t) = E_a \sin(\omega t + \beta)$, where

$$\sin \beta = -\nu_D^{(\text{ac})} \left[\left(\nu_D^{(\text{ac})} \right)^2 + \left(1 + \frac{M_D^{(\text{ac})}}{m_e} \right)^2 \omega^2 \right]^{-1/2}.$$

The relation between amplitudes of the field and velocity

$$E_a = \frac{m_e}{e} v_a \sqrt{\left(\nu_D^{(\text{ac})} \right)^2 + \left(1 + \frac{M_D^{(\text{ac})}}{m_e} \right)^2 \omega^2} \quad (19)$$

can be considered as the balance equation for the amplitudes, where $\nu_D^{(\text{ac})}$ and $M_D^{(\text{ac})}$ are rather complicated functions of v_a , ω and the ripplon damping. The right side of Eq. (19) as a function of v_a has a maximum. The balance of forces is impossible if the field amplitude E_a exceeds this maximum. Therefore, this ac treatment is an extension of the dc decoupling model where the current was fixed to a constant value.

It is important that in the ac theory, the dimple mass $M_D^{(\text{ac})}$ enters the balance of forces equation for amplitudes, and at high enough frequencies it can affect WS decoupling.

C. Comparison with results of the given-filed regime

Naturally, there is a question: can we rely on the results of the given-current treatment when considering a given-field regime? To analyze this problem let us consider the given-field regime and investigate the delicate behavior of functions $M_D^{(\text{ac})}$ and $\nu_D^{(\text{ac})}$ near subharmonic resonances ($\omega \sim \omega_g/2$) established previously^{13,14} for the inverse treatment. This frequency range is important for understanding the subharmonic phonon-ripplon coupling¹³. A comparison of low-frequency ($\omega \rightarrow 0$) results is presented in the next Subsection.

Of course, in the given-field regime, the equation of motion [Eq. (3)] cannot be solved exactly. Still, we can expand the exponential functions entering Eqs. (1) and (2) in power series restricting our consideration to the first nonlinear terms. Now, the driving field is fixed to a harmonic function $E(t) = E_a \cos(\omega t)$, while $u(t)$ can be represented as a Fourier series

$$u(t) = \sum_{k=-\infty}^{\infty} u_k e^{ik\omega t}. \quad (20)$$

We shall assume that the amplitudes of higher harmonics $|u_k|$ decrease fast with $|k|$. By definition, the driving field has only one harmonic ($k = \pm 1$) with $E_1 = E_{-1} = E_a/2$.

Using Eq. (20), we can find the equation of motion of the coupled WS-DL system for a weak nonlinearity

$$-\omega^2 \mathcal{Z}_k u_k + \chi_k^{\text{NL}} = \frac{e E_k}{m_e}, \quad (21)$$

where χ_k^{NL} is the contribution from nonlinear terms

$$\begin{aligned} \chi_k^{\text{NL}} = & \frac{1}{6} \sum_{\mathbf{g}} \Gamma_g \omega_g^4 g^2 \frac{g_x^4}{g^4} \left(\frac{1}{\Delta_{k,g}} - \frac{1}{\Delta_{0,g}} \right) \sum_{n,l} u_n u_l u_{k-n-l} + \\ & + \frac{1}{2} \sum_{\mathbf{g}} \Gamma_g \omega_g^4 g^2 \frac{g_x^4}{g^4} \sum_l u_{k-l} \left(\frac{1}{\Delta_{k-l,g}} - \frac{1}{\Delta_{l,g}} \right) \sum_n u_n u_{l-n}, \end{aligned} \quad (22)$$

and we had used the following notations: $\Delta_{k,g} = \omega_g^2 - k^2 \omega^2 + 2ik\omega\gamma_g$,

$$\mathcal{Z}_k(\omega) = k^2 + \sum_{\mathbf{g}} \Gamma_g \left(\frac{\omega_g}{\omega} \right)^2 \frac{k^2 \omega^2 - 2ik\omega\gamma_g}{\omega_g^2 - k^2 \omega^2 + 2ik\omega\gamma_g}. \quad (23)$$

The appearance of only cubic terms in χ_k^{NL} is caused by the fact that in the integrand of Eq. (4) we have to expand the sine function. In the limit $\gamma_g \rightarrow 0$, the quantity $\mathcal{Z}_1(\omega)$ represents the linear response function $\mathcal{Z}_1(\omega) \rightarrow 1 + M_D^{(\text{ac})}(\omega)/m_e$ which is frequently used for the description of electron-rippion resonances^{1,21} and phonon-rippion coupling. Note that in the linear ac theory, the dimple-mass function $M_D^{(\text{ac})}(\omega)$ has a resonance at $\omega \rightarrow \omega_g$, which is the reason for phonon-rippion coupling³, and it changes its sign for $\omega > \omega_g$. The negative values of $M_D^{(\text{ac})}(\omega)$ represent an oscillatory response of the DL: the WS and DL oscillate out of phase.

Consider the nonlinear equation for the first harmonic u_1 . Assuming that higher harmonics u_k decrease fast with k , one can find the first nonlinear correction to the effective mass function $M_D^{(\text{ac})}(\omega)$

$$\begin{aligned} \frac{\delta M_D}{m_e} = & \frac{|u_1^{(0)}|^2}{2} \sum_{\mathbf{g}} \Gamma_g \frac{g_x^4 \omega_g^4}{g^2 \omega^2} \times \\ & \times \text{Re} \left(\frac{\Delta_{-1,g} - \Delta_{2,g}}{\Delta_{2,g} \Delta_{-1,g}} - 3 \frac{\omega_g^2 - \Delta_{1,g}}{\Delta_{1,g} \omega_g^2} \right), \end{aligned}$$

where $u_1^{(0)}$ is the solution of the linear equation. Using the definitions of Eq. (15) and neglecting ripplon damping, the dimensionless mass function can be written as

$$\mathcal{M}_{\text{ac}}(v'_{a,0}) = \frac{1}{1 - (\omega')^2} \left\{ 1 + \frac{3}{2} \frac{(v'_{a,0})^2}{[1 - (2\omega')^2]} \right\} \quad (24)$$

where $v'_{a,0} = 2u_1^{(0)}\omega/v_{|g_x|} = u_a^{(0)}\omega/v_{|g_x|}$, and $u_a^{(0)}$ is the linear approximation for the amplitude of the first harmonic of $u(t)$. Already from this equation, one can see that the nonlinear correction to \mathcal{M}_{ac} leads to the subharmonic resonance of the dimple mass at $\omega \rightarrow \omega_g/2$, which agrees with the result found for the given-current regime. Higher nonlinear terms surely will lead to other subharmonic resonances at $\omega \rightarrow \omega_g/l$ (here $l = 3, 4, \dots$).

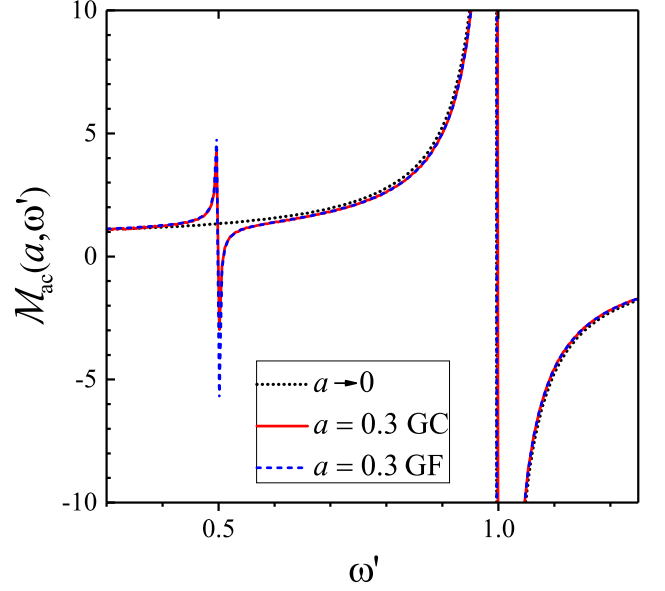


FIG. 1: The dimensionless dimple-mass function $\mathcal{M}_{\text{ac}}(a, \omega')$ versus frequency ω' calculated for the given-current (GC) and given-field (GF) regimes at a fixed value of the nonlinear parameter $a = |g_x| u_a^{(0)} = 0.3$. The exact solution of the GC regime was calculated at $\gamma'_g = 0.0025$, while the asymptote of the GF regime [Eq. (24)] has $\gamma'_g = 0$.

Another nonlinear effect which can be seen from Eq. (24) is that the velocity amplitude $v'_{a,0}$ reduces the first harmonic resonance ($\omega \rightarrow \omega_g$) because the second term in curly brackets becomes negative if $\omega' \simeq 1$. Eventually this reduction can change the sign of resonant variations of $\mathcal{M}_{\text{ac}}(v'_{a,0}, \omega')$.

The comparison of the exact solution of the given-current regime [Eq. (17)] with the approximation [Eq. (24)] found for the given-field regime is shown in Fig. 1. Following notations of Ref. 14, we shall use the dimensionless parameter $a = |g_x| u_a^{(0)} \equiv |g_x| v_{a,0}/\omega$ describing the strength of nonlinearity because it enters the exponential functions of Eqs. (1) and (2). The exact result of Eq. (17) shown in Fig. 1 by the solid (red) line was calculated for $a = 0.3$ and a small but finite damping coefficient ($\gamma'_g = 0.0025$) because the integrand represents a highly oscillating function. The dashed (blue) line represents the approximation of Eq. (24) taken at the same value of the nonlinear parameter a . One can see that the approximate form of the given-field regime is so close to the exact form of the given-current regime that it is impossible to distinguish the two lines except for a small vicinity of $\omega' = 1/2$ where the ripplon damping affects the exact solution.

At a substantially larger value of the nonlinear parameter $a = 1$, the deviations of the approximate equation of the given-field regime from the exact result of the given-current regime become noticeable as indicated in

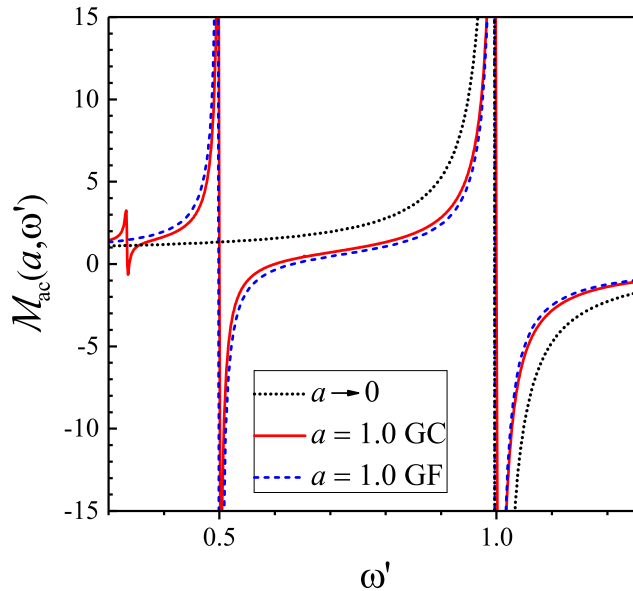


FIG. 2: The dimensionless dimple-mass function $\mathcal{M}_{\text{ac}}(a, \omega')$ versus frequency ω' calculated for the given-current (GC) and given-field (GF) regimes at a fixed value of the nonlinear parameter $a = |g_x| u_a^{(0)} = 1$.

Fig. 2. The approximate form leads to a bit stronger nonlinear effect. Nevertheless, the approximate form is not far away from the exact result except for the vicinity of $\omega' = 1/3$, where higher nonlinear terms become important according to the red-solid line of Fig. 2.

In the given-field regime, finding higher terms of the expansion of $\mathcal{M}_{\text{ac}}(v'_a, 0)$ in power series is a very difficult task. Still, we can find a better approximation if the second term in curly brackets of Eq. (24) is improved as

$$\frac{3}{2} \frac{(v'_{a,0})^2}{[1 - (2\omega')^2]} \left[1 + \frac{5}{4} \frac{(v'_{a,0})^2}{[1 - (3\omega')^2]} \right].$$

This rule follows from the expansion of the low-frequency expression for $\mathcal{M}_{\text{ac}}(v'_a)$ found for the given-current regime in the next Subsection. This improvement makes the dashed line very close to the solid line of Fig. 2 even for $a = 1$. The algorithm of finding series expansion of Eq. (17) allows us to calculate the dimple mass at a necessary accuracy even for zero ripplon damping.

The appearance of maxima of the function \mathcal{M}_{ac} at subharmonic frequencies $\omega \rightarrow \omega_g/l$ (here $l = 2, 3, \dots$) is quite obvious even from Eq. (22) obtained for the given-field regime. Therefore, we conclude that the results obtained for $M_D^{(\text{ac})}(v_a)$ and $\nu_D^{(\text{ac})}(v_a)$ in the given-current regime can quite well describe the respective quantities measured in the given-field regime at medium frequencies $\omega < \omega_{g1}$. The case of a much low frequency $\omega \ll \omega_{g1}$ is considered below.

III. LOW-FREQUENCY LIMIT OF THE NONLINEAR AC TRANSPORT

Experiments on nonlinear WS transport over liquid helium usually were conducted for an ac driving potential. In this case, field-velocity characteristics were presented for time-averaged quantities or amplitudes. Therefore, we expect that results obtained using a nonlinear dc model may not be applied to the data found in an ac experiment. Partly this problem was analyzed in Refs.^{12,14}. Here we would like to investigate the low-frequency limit of the nonlinear ac transport of the WS over superfluid ^4He at $T < 0.4\text{K}$. In this case, ripplon damping is extremely small and the ratio $\gamma_{g1}/\omega_{g1} < 10^{-4}$ (here g_1 is the smallest reciprocal lattice vector). At the same time the frequency of the driving potential in experiments on the WS transport is rather low, and a typical value of the ratio $\omega/\omega_{g1} \sim 10^{-3}$. Therefore, it is important to find the asymptotic behavior of field-velocity characteristics of the ac WS transport in the limit of low frequencies and damping.

Firstly, consider the limiting case of zero damping. Then, the low-frequency asymptote of the dimensionless function $\mathcal{M}_{\text{ac}}(v'_a, \omega', \gamma'_g)$ defined above in Eq. (17) can be found in an analytical form

$$\mathcal{M}_{\text{ac}}(v'_a) \rightarrow \frac{\theta(1 - |v'_a|)}{[1 - (v'_a)^2]^{3/2}}, \quad (25)$$

where we use the absolute-value symbol because the definition of v'_a contains g_x which can change its sign. One can notice that this equation differs substantially from the result of the dc theory given in Eq. (10) and taken at $\gamma'_g = 0$. The difference is caused by the fact that $\mathcal{M}_{\text{ac}}(v'_a)$ is a time-averaged quantity (a Fourier transform).

It is important to note that expanding Eq. (25) in $(v'_a)^2$ and neglecting the terms of a higher power we obtain the result which coincides with Eq. (24) found for the given-field regime and taken at $\omega' = 0$. Thus, we proved the agreement (even numerical) between the solutions found in two opposite regimes in the wide range of frequencies which includes the limit $\omega \rightarrow 0$. The result of Eq. (25) indicates also that a dc transport model cannot always be applied to the time-averaged quantities or amplitude data of an ac transport experiment. Another important consequence of Eq. (25) is that it allows us to formulate the algorithm for the series expansion of Eq. (17) in $(v'_a)^2$ valid for a finite frequency and zero ripplon damping, as discussed in the preceding Subsection.

It is instructive to see how $\mathcal{M}_{\text{ac}}(v'_a, \omega', \gamma'_g)$ of Eq. (17) approaches the asymptote given in Eq. (25) with lowering frequency ω . The results of calculations based on Eq. (17) are shown in Fig. 3 together with the asymptote. We found that at low velocities $v'_a < 1$ and ω' the exact form of $\mathcal{M}_{\text{ac}}(v'_a, \omega', \gamma'_g)$ coincides with the asymptote indicated by the red dash-dotted line. Deviations from this line, which appear in the vicinity of the BC condition $v_a \simeq v_{|g_x|}$, increase strongly with ω' . One can

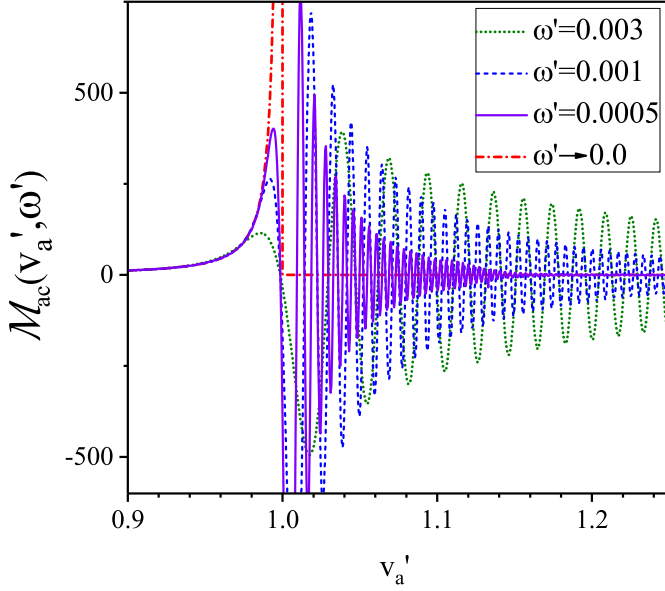


FIG. 3: The dimensionless dimple-mass function $\mathcal{M}_{ac}(v'_a, \omega')$ versus the velocity amplitude v'_a calculated for different frequencies. The damping parameter γ'_g is fixed to 0.0025.

see that the BC threshold for the dimple mass is strongly affected by the finite frequency of the driving field. At a fixed $\gamma'_g = 0.0025$ the maximum of the threshold decreases with increasing ω' . A remarkable behavior of the mass function $\mathcal{M}_{ac}(v'_a)$ is seen above the BC threshold: in this range, it approaches the asymptote of Eq. (25) in a highly oscillating way. Moreover, at maxima of these oscillations, the dimple mass can be even larger than at the BC maximum. This means that above the BC threshold the WS and DL go through multiple decoupling and recoupling processes.

The BC threshold exists not only for the smallest g ; it exists also for all other reciprocal lattice vectors which have a nonzero component along the velocity vector. Therefore, in the limiting case $\omega' \rightarrow 0$, the dimple mass $M_D^{(ac)}$ has many sharp peaks as illustrated in Fig. 4 by the blue-dotted line. At a rather low frequency $\omega = 10^4 \text{ s}^{-1}$ and $\gamma'_{g1} = 0.003$, the calculated line (olive-dashed) has finite maxima and negative minima just above the BC conditions. It should be noted that negative values of $M_D^{(ac)}$ simply mean the oscillatory response of the DL similar to that discussed above just after Eq. (23). For the substantially higher frequency $\omega = 10^6 \text{ s}^{-1}$, the position of maxima (except for the first one) and decoupling processes have no relation to the BC conditions. The further increase in frequency ($\omega = 10^7 \text{ s}^{-1}$) strongly suppresses the BC effect resulting in a smooth line (dash-dotted purple).

Consider now the nonlinear kinetic friction described by the functions $\nu_D^{(ac)}$ and \mathcal{N}_{ac} . In the limiting cases $\omega' \rightarrow 0$ and $\gamma'_g = 0$, the asymptotic behavior of $\mathcal{N}_{ac}(v'_a)$

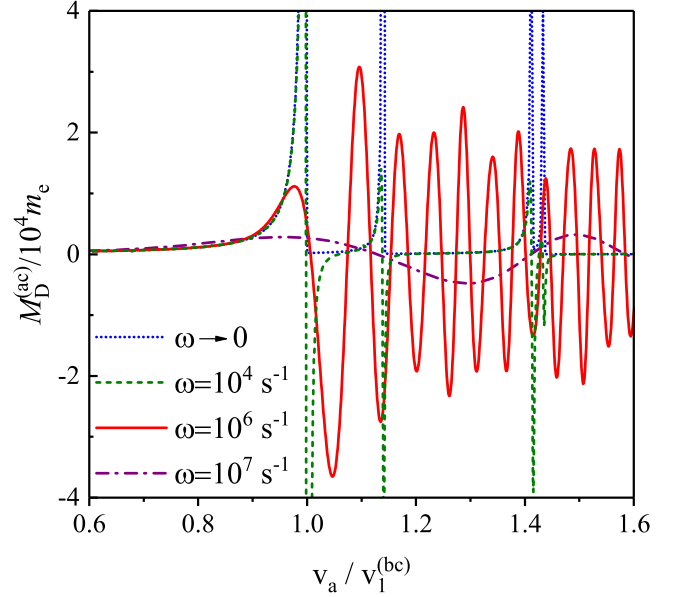


FIG. 4: The dimple-mass $M_D^{(ac)}$ normalized versus the velocity amplitude v_a calculated for $n_e = 5 \cdot 10^8 \text{ cm}^{-2}$, $T = 0.15 \text{ K}$ and different frequencies. The damping parameter γ'_{g1}/ω_{g1} is fixed to 0.003.

defined in Eq. (18) is found as

$$\mathcal{N}_{ac}(v'_a) \simeq \frac{2\theta(|v'_a| - 1)}{(v'_a)^2 \sqrt{(v'_a)^2 - 1}}. \quad (26)$$

According to this equation, the BC peak of $\mathcal{N}_{ac}(v'_a)$ has a strongly asymmetric shape which is in contrast with the result of the dc model given in Eq. (8). A comparison with the given-field regime cannot be given because $\mathcal{N}_{ac}(v'_a)$ of Eq. (26) differs from zero only at high-velocity amplitudes $|v'_a| \geq 1$. The evolution of the exact function $\mathcal{N}_{ac}(v'_a)$ calculated for a fixed $\omega' = 0.001$ and several values of the damping parameter γ'_g is shown in Fig. 5. An increase in γ'_g reduces the BC-threshold maximum and the amplitude of oscillations in the tail region. A different behavior of $\mathcal{N}_{ac}(v'_a)$ is obtained for a fixed $\gamma'_g = 0.0025$ with increasing the frequency parameter ω' as shown in Fig. 6. The BC maximum is reduced by an increase in ω' , but the amplitude of oscillations and their period in the tail region become larger.

The typical behavior of $\nu_D^{(ac)}(v_a)$ is illustrated in Fig. 7 for different frequencies $\omega \ll \omega_{g1}$. It is remarkable that above the BC threshold $\nu_D^{(ac)}(v_a)$ is finite (except for BC points of larger \mathbf{g}) even for zero damping (black dotted line). This greatly distinguishes the ac theory from the dc model, where $\nu_D^{(dc)}(v_a)$ is zero except for the BC δ -peaks if $\gamma_g = 0$. The increase of frequency up to 10^4 s^{-1} (blue dashed line) makes the transition through the BC conditions smooth. Away from the BC critical points, this line follows the asymptote of Eq. (26). At even higher

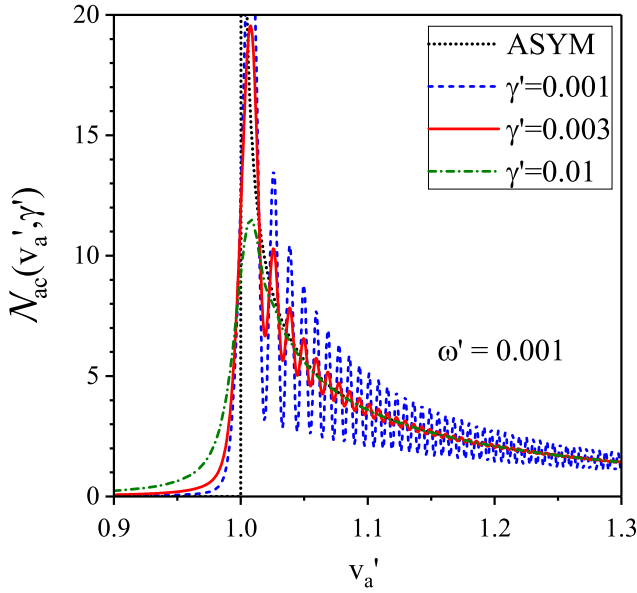


FIG. 5: The dimensionless function $\mathcal{N}_{ac}(v'_a, \gamma')$ versus the velocity amplitude v'_a calculated for a fixed frequency $\omega' = 0.001$ and different values of the damping parameter $\gamma' = \gamma_g/\omega_g$. The black dotted line represents the asymptote (ASYM) of Eq. (26).

$\omega = 10^5 \text{ s}^{-1}$ the line (red solid) oscillates near the the asymptotic line of the limiting case $\omega = 0$. The amplitude of these oscillations is substantial only in the vicinity of the first BC peak, and it decreases for higher velocities where this solid line is close to the blue-dashed line and the asymptote of Eq. (26). The higher frequency $\omega = 10^6 \text{ s}^{-1}$ (purple dash-dotted line) makes the oscillations more pronounced and shifts strongly the BC maximum to the right. At $\omega = 10^7 \text{ s}^{-1}$, (olive dash-dot-dotted line) the BC threshold is practically destroyed.

IV. DISCUSSIONS AND CONCLUSIONS

The results obtained for the low-frequency limit indicate that the BC emission of surface waves by the WS remains to be an important feature of electron transport on superfluid helium even under ac conditions. For low frequencies ($10^4 \text{ s}^{-1} \leq \omega \leq 10^5 \text{ s}^{-1}$), the dimple mass $M_D^{(ac)}$ and the effective collision frequency $\nu_D^{(ac)}$ caused by electron interaction with a surface dimple increase sharply when velocity amplitude v_a approaches $v_1^{(bc)}$. Therefore, the BC effect should restrict the velocity and current amplitudes with a moderate increase of the amplitude of the driving electric field. The typical values of $\nu_D^{(ac)}$ induced by the motion of surface dimples and shown in Fig. 7 are much larger than the rate of electron collisions with thermally excited ripples ν_e . Therefore, the ordinary drag force $-m_e \nu_e v_a \cos(\omega t)$ acting on an electron can be

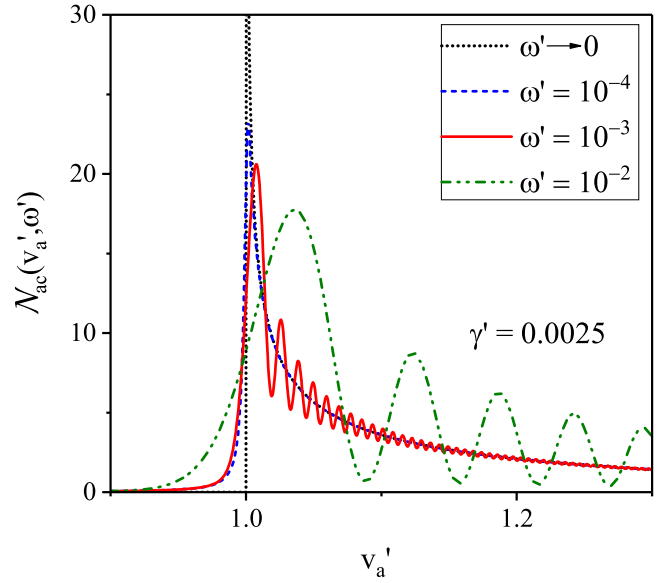


FIG. 6: The dimensionless function $\mathcal{N}_{ac}(v'_a, \omega')$ versus the velocity amplitude v'_a calculated for a fixed damping parameter and different frequencies ω' . Other notations are the same as in Fig. 5.

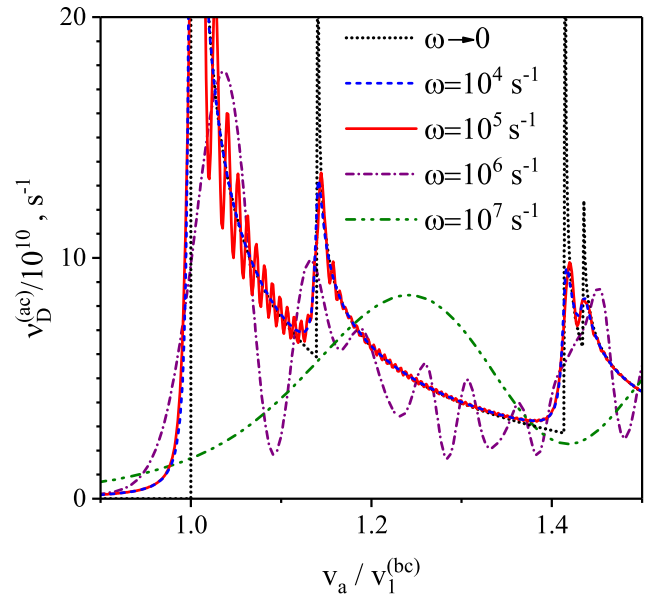


FIG. 7: The effective collision frequency caused by electron interaction with a surface dimple $\nu_D^{(ac)}$ versus the velocity amplitude v_a calculated for $n_e = 5 \cdot 10^8 \text{ cm}^{-2}$, $T = 0.15 \text{ K}$, and different frequencies. The damping parameter γ_{g1}/ω_{g1} is fixed to 0.003.

neglected in the force balance equation.

An increase in the frequency of the signal differently affects the BC maxima of $M_D^{(ac)}(v_a)$ and $\nu_D^{(ac)}(v_a)$: in the first case, they are displaced left to lower velocity amplitudes, while for $\nu_D^{(ac)}(v_a)$ they are displaced right to higher v_a . Another important distinction to be noticed here is that the BC peaks of $M_D^{(ac)}$ and $\nu_D^{(ac)}$ have opposite asymmetries (with respect to $v_a = v_1^{(bc)}$) which become more prominent at low driving frequencies. For the first BC resonance, with $\omega \rightarrow 0$ and $\gamma_g \rightarrow 0$, these quantities approach zero at the opposite sides with respect to the critical point $v_a = v_1^{(bc)}$. Thus, the behaviors of the major transport properties of the WS obtained here for ac conditions are in contrast with the simple treatment of a stationary motion ($v = \text{const}$) of electrons¹¹.

Another interesting effect obtained above is the very high values of the dimple mass $M_D^{(ac)}(v_a)$ appeared at the BC maximum and above it ($v_a > v_1^{(bc)}$) at oscillation maxima. These values are about two orders of magnitude (!) larger than the equilibrium dimple mass $M_D^{(ac)}(0)$. Therefore, the dimple mass should be taken into account in the balance of forces equation even for low frequencies $\omega \ll \omega_{g_1}$.

To obtain the field-velocity characteristic for the ac driving we have used the balance-of-amplitudes equation given in Eq. (26). The results of the calculations are shown in Fig. 8. Since we are considering the low-frequency limit, the dependence $E_a(v_a)$ is very similar to the dependence $\nu_D^{(ac)}(v_a)$ illustrated in Fig. 7. Important distinctions are found in the region $v_a < v_1^{(bc)}$. One can see that in this region an increase in the frequency of the signal strongly affects the field amplitude E_a related to a velocity amplitude v_a . In the opposite region, $E_a(v_a)$ varies in a quite oscillating way. Still, for the typical value $\omega = 10^5 \text{ s}^{-1}$, the amplitude of oscillations is small, and at average $E_a(v_a)$ is remarkably close to the line calculated for the limiting case $\omega \rightarrow 0$ under ac conditions.

The results presented in Fig. 8 are found for amplitudes of the major harmonics of the electric field and velocity. For a strong nonlinearity, the actual dependence of $v(t)$ can differ substantially from the simple cosine function because of the presence of higher harmonics appeared in the given-field regime. These harmonics can affect the shape of current oscillations, as was found in the time-resolved measurements¹⁷. In this experiment, at a strong driving potential amplitude, the current oscillations obtain a shape with long-flat extrema because of the BC effect (the velocity amplitude cannot exceed $v_1^{(bc)}$). Then, at substantially larger driving amplitudes the cosine-like shape of the current is almost restored with some remarkable oscillatory features observed in the vicinity of current extrema¹⁷.

For driving frequencies $\omega \ll \omega_{g_1}$, the DL adiabatically follows the WS motion changing its shape with increasing velocity. In this regime, WS-DL instability can happen

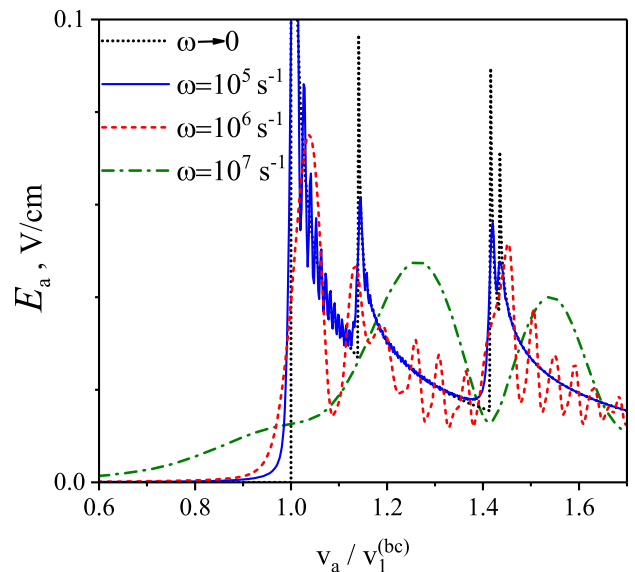


FIG. 8: Field-velocity characteristics for amplitudes calculated under ac conditions with different frequencies. Other parameters are the same as in Fig. 7.

according to the decoupling model. Regarding possible sliding of the WS over the nearly unchanged DL, the analysis of Eqs. (1) and Eqs. (2) indicates that it can happen if electron acceleration is high enough. The driving field should be changing fast within a time scale smaller than $\omega_{g_1}^{-1}$, which makes the process highly nonadiabatic. It should be noted that in experiments on WS decoupling¹⁶, the time scale of the driving field increase was comparable with the inverse of the ripplon frequency. At such conditions, the sliding model can be relevant to the sharp velocity jump observed.

In summary, we have investigated the ac nonlinear transport of the 2D Wigner solid over the free surface of superfluid ⁴He employing two different approaches. The first approach is formulated for the given-field regime. In this case, the nonlinear integro-differential equation of motion is solved approximately taking into account only the nonlinear terms of the lowest order. In the second approach, the current is assumed to be fixed to a simple harmonic function (the given-current regime), while the major harmonic of the driving field is found in an exact form and expressed in terms of the nonlinear dimple mass function and the effective collision frequency caused by electron interaction with the DL. Remarkably, for the lowest nonlinear approximation, both approaches lead to the same results in a wide range of driving frequencies. This means that the exact results found employing the given-current regime can be used for the description of the time-averaged measurements performed for the given-field regime as well.

Under ac driving conditions, we found that the dimple mass and the effective collision frequency as func-

tions of the velocity amplitude are increased strongly by the BC effect in a way which differs from that established previously using dc models. The BC maxima of the field-velocity characteristic calculated for amplitudes obtain an asymmetrical shape, whose parameters are strongly affected by the frequency of the signal and ripplon damping. For typical driving frequencies (lower or

about 10^5 s^{-1}), the field-velocity characteristic remarkably varies near a universal line calculated for the limiting case $\omega \rightarrow 0$ and zero damping. The nonlinear dimple mass has only a weak influence on the field-velocity characteristics. Still, in the given-current regime, it can be very large even far above the BC threshold.

-
- * E-mail: monarkha@ilt.kharkov.ua
- ¹ Yu.P. Monarkha and K. Kono, *Two-Dimensional Coulomb Liquids and Solids* (Springer-Verlag, Berlin, 2004).
 - ² Yu.P. Monarkha and V.B. Shikin, *Zh. Eksp. Teor. Fiz.* **68**, 1423 (1975) [*Sov. Phys. JETP* **41**, 710 (1975)].
 - ³ D.S. Fisher, B.I. Halperin, and P.M. Platzman, *Phys. Rev. Lett.* **42**, 798 (1979).
 - ⁴ C.C. Grimes and G. Adams, *Phys. Rev. Lett.* **42**, 795 (1979).
 - ⁵ R. Giannetta and L. Wilen, *Solid State Commun.* **78**, 199 (1991).
 - ⁶ K. Shirahama and K. Kono, *Phys. Rev. Lett.* **74**, 781 (1995).
 - ⁷ V. Sivokon', V. Dotsenko, Yu. Kovdrya, and V. Grigor'ev, *J. Low Temp. Phys.*, **111**, 609 (1998).
 - ⁸ K. Shirahama and K. Kono, *J. Low Temp. Phys.* **104**, 237 (1996).
 - ⁹ M.I. Dykman and Yu.G. Rubo, *Phys. Rev. Lett.* **78**, 4813 (1997).
 - ¹⁰ A. Kristensen, K. Djerfi, P. Fozooni, M.J. Lea, P.J. Richardson, A. Santrich-Badal, A. Blackburn, and R.W. van der Heijden, *Phys. Rev. Lett.* **77**, 1350 (1996).
 - ¹¹ W.F. Vinen, *J. Phys. Condens. Matter* **11**, 9709 (1999).
 - ¹² Yu.P. Monarkha and K. Kono, *Fiz. Nizk. Temp.*, **35**, 459 (2009) [*Low Temp. Phys.*, **35**, 356 (2009)].
 - ¹³ Yu.P. Monarkha, *Europhys. Lett.*, **118**, 67001 (2017).
 - ¹⁴ Yu.P. Monarkha, *Fiz. Nizk. Temp.*, **44**, 379 (2018) [*Low Temp. Phys.*, **44**, 286 (2018)].
 - ¹⁵ D. G. Rees, N. R. Beysengulov, J.-J. Lin, and K. Kono, *Phys. Rev. Lett.*, **116**, 206801 (2016).
 - ¹⁶ D. G. Rees, S.-S. Yeh, B.-C. Lee, S. K. Schnyder, F. I. B. Williams, J.-J. Lin, and K. Kono, *Phys. Rev. B* **102**, 075439 (2020).
 - ¹⁷ S. Zou, D. Konstantinov, and D.G. Rees, *Phys. Rev. B* **104**, 045427 (2021).
 - ¹⁸ A. A. Johansson and S. Stafstrom, *Phys. Rev. B* **69**, 235205 (2004).
 - ¹⁹ N.-H. Ge, C. Wong, R. Lingle, J. McNeill, K. Gaffney, and C. Harris, *Science* **279**, 202 (1998).
 - ²⁰ P. Gaal, W. Kuehn, K. Reimann, M. Woerner, T. Elsaesser, and R. Hey, *Nature (London)* **450**, 1210 (2007).
 - ²¹ Yu.P. Monarkha and V.E. Syvokon, *Fiz. Nizk. Temp.*, **38**, 1355 (2012) [*Low Temp. Phys.*, **38**, 1067 (2012)].